Electrostatics, proton sensor and networks governing the gating transition in GLIC, a proton-gated pentameric ion channel

Haidai Hu[1,2], Kenichi Ataka[3], Anais Menny[4], Zaineb Fourati[1], Ludovic Sauguet[1], Pierre-Jean Corringer[4], Patrice Koehl[5], Joachim Heberle[3] and Marc Delarue[1,&]

1. Unité Dynamique Structurale des Macromolécules, Institut Pasteur, and UMR 3528 du CNRS, 25 rue du Dr Roux, 75015 Paris, France. 2. Paris Sorbonne Université, Campus Pierre and Marie Curie, Paris 6, 75006 Paris, France. 3. Department of Physics, Experimental Molecular Biophysics, Freie Universität Berlin, Arnimallee 14, 14195 Berlin, Germany. 4. Unité Récepteurs-canaux, Institut Pasteur, and UMR 3571 du CNRS, 25 rue du Dr Roux, 75015 Paris, France. 5. Department of Computer Science, Genome Center, UC Davis, Davis, CA 94520, USA & Corresponding author Marc Delarue, Institut Pasteur, 25 rue du Dr Roux, 75015 Paris, France E-mail: marc.delarue@pasteur.fr Tel: +33 1 45 68 86 05

Submitted to Proceedings of the National Academy of Sciences of the United States of America

The pentameric ligand-gated ion channel (pLGIC) from *Gloeobacter violaceus* (GLIC) has provided insightful structure-function views on the permeation process and the allosteric regulation of the pLGICs family. However, GLIC is activated by pH instead of a neurotransmitter and a clear picture for the gating transition driven by protons is still lacking. We used an electrostatics-based (FD-DH) method to predict the acidities of all aspartic and glutamic residues in GLIC, both in its active and closed-channel states. Those residues with a predicted pKa close to the experimental pH_{50} were individually replaced by alanine and the resulting variant receptors were titrated by ATR-FTIR spectroscopy. E35, located in front of Loop F far away from the orthosteric site, appears as the key proton sensor with a measured individual pKa at 5.8. In the GLIC open conformation, E35 is connected through a water-mediated hydrogen-bond network first to the highly conserved electrostatic triad R192-D122-D32 and then to Y197-Y119-K248, both located at ECD-TMD interface. The second triad controls a cluster of hydrophobic side-chains from the M2-M3 Loop that is remodeled during the gating transition. We solved 12 crystal structures of GLIC mutants, 6 of them being trapped in an agonist-bound but non-conductive conformation. Combined with previous data, this reveals two branches of a continuous network originating from E35 that reach, independently, the middle transmembrane region of two adjacent subunits. We conclude that GLIC's gating proceeds by making use of Loop F, already known as an allosteric site in other pLGICs, instead of the classical orthosteric site.

Pentameric ligand-gated ion channel | pH activation | Proton sensor | Electrostatic networks | Allosteric modulation

Introduction

Pentameric ligand-gated ion channels (pLGICs), also known as Cys-Loop receptors in animals[1], or, more recently, Pro-loop receptors[2], mediate rapid signal transduction in the central and peripheral nervous systems[1]. Activation of these receptors is favored by the binding of agonist(s) in the extracellular domain (ECD), which lowers the activation energy between closed and open states[3]. This leads to a global allosteric conformational change and promotes the opening of the transmembrane domain (TMD) ion channel pore. Dysfunction of pLGICs can cause severe nervous-system diseases and conditions such as Alzheimer's disease, Parkinson's disease, epilepsy, and alcohol dependence. They are the targets of several important therapeutic compounds such as general anesthetics, barbiturates and benzodiazepines, whose structures of complexes with a pLGIC are reviewed in [4].

Available structural information on this family was derived from a number of prokaryotic and eukaryotic channels[5]–[13]. Despite substantial diversity of sequences, structural information shows high conservation of tertiary and quaternary architectures between eukaryotic receptors and their bacterial homologs. Besides the covalent link between ECD and TMD through the pre-M1 region, the ECD-TMD interface comprises with four highly conserved loop regions: the β1-β2 loop, the Loop F, the Pro-loop and the M2-M3 loop[1], [14] (**Fig. 1A inset**). Of all pLGICs, the prokaryotic ELIC from *Erwinia chrysanthemi* and GLIC from *Gloeobacter violaceus* stand out as the subjects of many structure-function relationship studies. Notably, GLIC has been captured in four different states. Following the first apparently open/active state of GLIC crystallized at pH 4.0[13], [15], several proton-bound but non-conducting forms have been solved, which have been designated as 'Locally Closed' states (LC)[16]–[18]. Among those LC forms, which all display an unfolding of the C-terminus of the M2 helix and a change of its orientation that closes the pore but have different conformations of M2-M3 loop, one of them (LC2) has been recently suggested to be a pre-active state, an intermediate state along the transition pathway from the resting state to the active state[19]. The closed/resting state of GLIC was solved at neutral pH[20]. Finally, the structure of a putative desensitized state of GLIC has also been reported[21]. In addition, GLIC has been extensively used to characterize the binding properties of important pharmacological reagents, such as propofol[22], bromoform[23], [24], ethanol[23], [25] and barbiturates[26], while ELIC has also been used for the structural

Significance

Several classes of membrane ion channels are sensitive to the intracellular or extracellular proton concentration. However, the detailed mechanism of channel gating induced by protonation proves in general difficult to address. Here we use a combined computational and experimental approach to identify the proton sensor in the pentameric proton-gated ion channel GLIC. Further electrophysiology and crystallography data help delineate the mechanism of the gating transition initiated by protonating this sensor, revealing that those positions that trap the receptor in a nonfunctional closed pore conformation build up a continuous network. Our results provide a novel approach to search for and identify proton sensors as well as networks of residues important for the gating transition in the pentameric ligand-gated channels family.

Reserved for Publication Footnotes

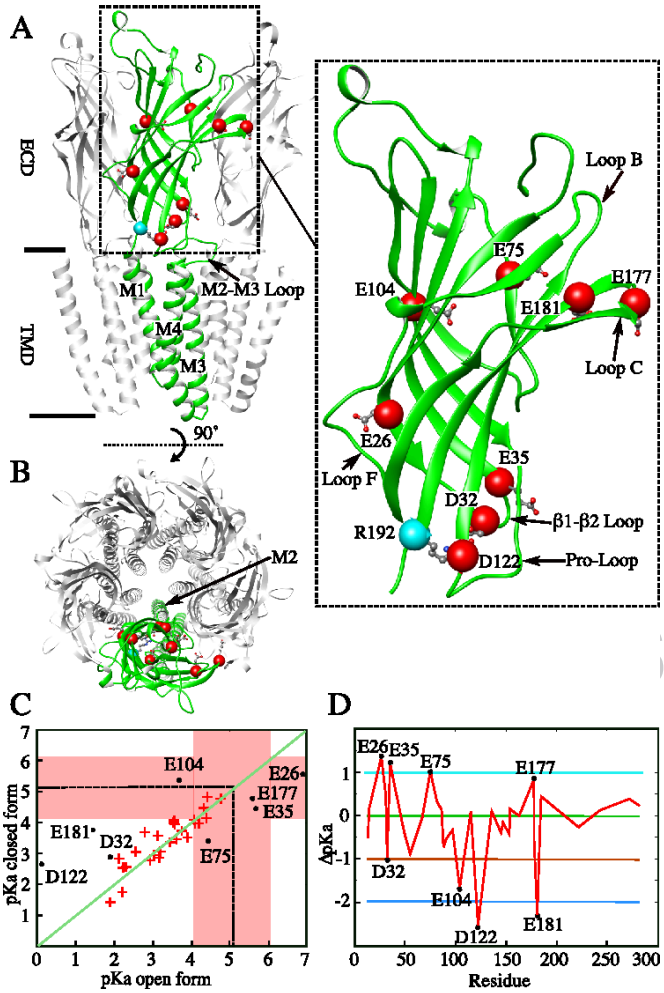

Fig. 1. Predictions of proton-sensing residues among all Glu and Asp in GLIC derived from electrostatic FD/DH calculations. (**A**) Cartoon representation of the open form of GLIC crystallized at pH 4. The front subunit is highlighted and shown in green. Asp and Glu residues predicted to have ΔpKa larger than 1 unit between the open and closed states are shown as sticks and their Cα atoms are shown as red van der Waals spheres (inset). Cα atom of R192 is shown as a cyan sphere. The black bars represent the plasma membrane level. (**B**) Top view of GLIC with color and representation of atoms identical to A. (**C**) Scatter plots for the predicted pKa values of all Asp (19 for each subunit) and Glu (16 for each subunit) for the open and closed forms of the receptor. Residues lying on the diagonal (green line) have predicted pKa values that are equal in the two forms. The pink region contains residues for which the protonation state is predicted to change at pH_{50} ± 1 (pH_{50} = 5.10 ± 0.20). (**D**) ΔpKa values, from the open to closed form, of Asp and Glu are plotted as a function of the residue number (red line).

characterization of the binding of general anesthetics and benzodiazepine molecules[27]–[29]. A number of biophysical methods such as EPR have also been applied to characterize GLIC conformations in solution. These methods, due to their inherent time scale, are likely to probe the desensitized state, whose structure is still highly debated, leading to some apparent disagreement in the interpretation of the experiments[30]–[33].

GLIC's channel is gated by proton(s) with pH_{50} = 5.1 ± 0.2, at which half the maximal current amplitude is reached. This contrasts with most human pLGICs, which are activated by neurotransmitter binding to a cavity in an inter-subunit interface in the ECD, mainly involving loops B and C (**Fig. 1A inset**). Various invertebrate pLGICs have been demonstrated to be directly responsive to pH[34]–[36]. Proton-gating has also been observed in ion channels that are not members of the pLGIC family, such as acid-sensing ion channels (ASIC) and some inward-rectifying potassium channels (Kir) [37], [38]. The mechanism of proton gating is in general very difficult to study as there are many candidates for the role of proton-sensing residues. In addition, protons are usually not directly seen by crystallography, precluding the possibility to ascertain which residue is protonated and which is not, even if the structure is known at high-resolution.

In this study, we performed a systematic and computer-aided survey of residues that can be qualified as proton sensors contributing to channel gating in GLIC, namely residues that change their protonation state during the conformational transition. Taking advantage of the knowledge of the structures of open/active and closed/resting forms of GLIC, we use the Finite Difference Poisson-Boltzmann/Debye-Hückel (FD/DH) to predict individual pKa values and to guide the search for the position of pH-sensing residues. FD/DH has been shown to be superior to classical FD-PB[39] for filtering candidate residues responsible for pH-induced channel gating. We then experimentally determined the *individual* pKa values of those residues that exhibit a strong change in the calculated pKa values between the two known states, by employing Attenuated Total Reflectance Fourier Transform Infra-Red Spectroscopy (ATR-FTIR). The assignment of the carboxylic side chain frequencies was performed by replacement of individual carboxylate residues by alanine and calculating the difference between the spectra of the wild-type and mutated receptors. We infer from these results that E35 accounts for proton sensing, in accordance with recent electrophysiology results[40].

We then extensively explored the environment of residue E35, located at the ECD-TMD interface with Loop F of the adjacent subunit, by site-directed mutagenesis, chemical labeling, electrophysiology and crystal structure analysis and found an interfacial hydrogen network mediated by water molecules which controls channel gating, in association with an additional layer made of an intra-subunit cluster of hydrophobic side-chains. Both networks are crucial for maintaining the channel open. These networks can be mapped further down to the middle pore region in two adjacent subunits by projecting on the structure of the active state of GLIC all known positions whose mutation results into an LC structure, namely a structure trapped before the transition to the active form.

Results

Poisson-Boltzmann electrostatics and the FD/DH method predict potential pH-sensing residues in GLIC

Activation of GLIC is triggered by lowering the pH from neutral to acidic values with a pH_{50} = 5.1 ± 0.2. Our goal is to identify those residues whose protonation will most profoundly affect the conformational transition between the closed and the open forms of the channel. These are likely to be either Asp, or Glu or His residues. There are 34 carboxylate residues in each subunit, along with 3 His residues. Here we focus on Asp and Glu as it has been shown elsewhere that His residues play no role in the gating transition[40]. It is expected that the pKa values of carboxylate residues that are essential to proton activation should be significantly shifted from their model pKa (Asp = 3.8-4.0; Glu = 4.2-4.4). However, this is a necessary but not sufficient condition to predict/identify the proton-sensing residues. Indeed, following Sazanavets and Warwicker[39], one can divide residues whose pKa values are shifted from their model pKa in two classes: pH-sensors and pH-coupled. Only the pH-sensors are expected to change ionization during the conformational change between the two forms, namely around pH_{50} ± 1, whereas proton-coupled residues are not[39].

Poisson-Boltzmann (PB) electrostatic calculations can predict individual pKa values of a protein with a known structure. FD/DH calculation is a refined Poisson-Boltzmann method that

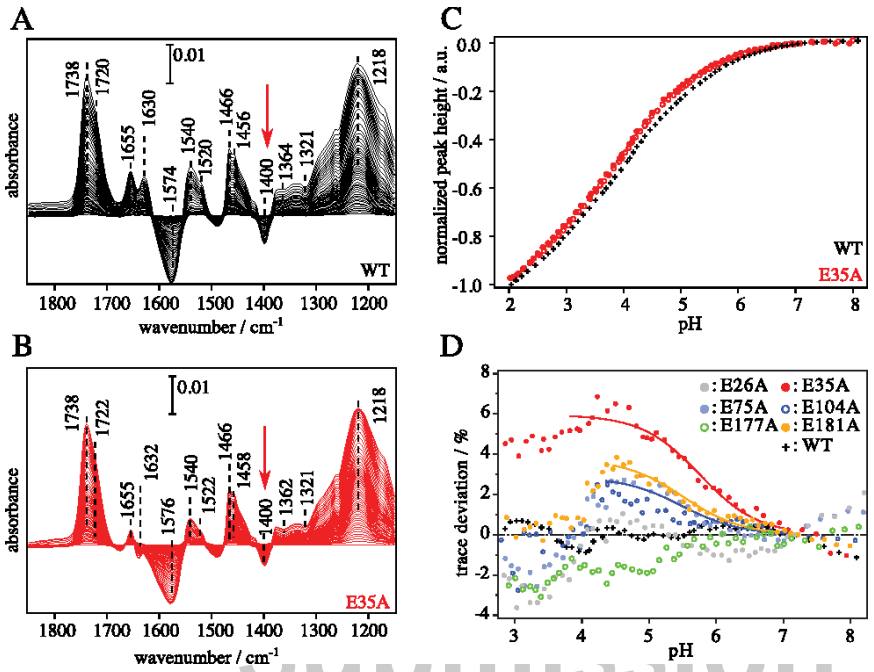

Fig. 2. pH-induced FTIR difference spectra of GLIC reconstituted in POPE/POPG lipids of (**A**) Wild-type GLIC and (**B**) the E35A mutant. Reference spectra were taken at pH = 7.0 and FTIR differences were recorded while the solution pH was continuously lowered. Negative peaks represent the structural components that were reduced after lowering the pH, while positive peaks represent the structural components that were gained by lowering the pH. (**C**) pH titration curves derived from the normalized intensities of the band at 1400 cm^{-1} (symmetric carboxylate vibration) of the wild-type (+) and of the E35A mutant (red). Open and filled symbols represent data from different experiments performed under identical conditions. (**D**) Deviations of the mutants' pH titration from the wild-type. The cross marker in black (+) represents trace deviation of wild-type between two different experiments, which sets the extent of the reproducibility error. The solid curves represent results of fitting the data points by the Henderson-Hasselbalch equation for E35A, E75A, E181A.

has been shown to be significantly better at predicting pH-sensing residues compared to normal FD-PB methods[39]. For charged and exposed residues the method takes into account both their intrinsic flexibility by sampling all possible rotamers and also the screening effect due to the surrounding salt by using the Debye-Huckel theory[39]. GLIC X-ray structures have been solved in both its open/active form (pH 4.0, PDB ID: 3EAM, 4HFI) and in its closed/resting form (pH 7.0, PDB ID: 4PQN) so that we can calculate pKa values in both forms.

The FD-DH analysis of all GLIC carboxylate protonatable residues shows that most have the same predicted pKa values in both states (**Fig. 1C** and **SI Appendix, Notes**), suggesting that they are not involved in pH sensing. Interestingly, five Glutamate residues, E26, E35, E75, E104, and E177, are predicted to change protonation state within one log of the functional pH_{50} and have a predicted pKa value significantly different in the two states (pink zone in **Fig. 1C**). E177 is located near the known agonist-binding site (Loop C), while E26, E35 and E75 are at the interface between two subunits. E104 is located close to a known positive allosteric modulator (PAM) binding site (**Fig. 1A inset**).

In comparison, the pKa values of D32, D122 and E181 differ substantially between the open and the closed forms ($\Delta pKa \geq 1$), but in a pH range distant from GLIC's pH_{50} (**Fig. 1C-D**), and are therefore more likely to be pH-coupled residues, rather than pH-sensing [39]. D32 and D122 are involved in strong electrostatic interactions with R192, which are highly conserved in almost all pLGIC, even in receptors that are not activated/modulated by pH changes[2]. Mutations at these positions often impair the expression of the receptors at the cell membrane or lead to total loss-of-function phenotypes (**SI Appendix, Table S1**). Therefore, they are not expected to play a role in proton sensing *per se* but rather to be essential for maintaining the structural integrity of the receptor. E181 is located in Loop C, which experiences a considerable conformational change between the two states and would be a good candidate for proton sensing (**SI Appendix, Fig. S2B**). However, its predicted pKa is not in the range of $pH_{50} \pm 1$. Furthermore, mutations of each protonatable residue in loop C show no or small effects on proton activation in the range of pH 7.0-4.0[41], [42]. Indeed, deleting the entire loop C or replacing it by 10 glycines does not affect pH activation of GLIC[17].

The output of FD-DH calculations contains a list of putative salt bridges and strong hydrogen bonds in the structure, along with their calculated energy. The strongest ion pairs (with an interaction energy around 9 kT in the open form, but 6 kT in the closed form) involve the triad R192, D122 and D32, a strongly conserved feature of all pLGICs[2]. Interestingly, the less-known triad made of Y197-Y119 within the same subunit and K248 of the next subunit is at the same energy level (8.5-9.5 kT). These two "triads", hereafter referred to as "primary" and "secondary" triads, respectively, are linked together by an interaction between Y197 and R192 of 4.8-5.2 kT in the open form (but not in the LC forms). The interactions between K248 and Y119 or Y197 are weakened in the closed form (**SI Appendix, Notes**).

To further characterize the potential candidates for pH-sensing (E26, E35, E75, E104, E177), titrations using FT-IR spectroscopy in combination with site-directed mutagenesis were performed to experimentally derive their *individual* pKa values, as these quantities cannot be derived easily from electrophysiology experiments. Other residues (D86, D88, E67, D97, E181 and E243) served as experimental controls (**SI Appendix, Fig. S3**).

Experimental determination of the individual pKa values of potential pH-sensing residues by ATR/FT-IR spectroscopy

FTIR spectroscopy of the pH-induced conformational transition of GLIC has been conducted using the ATR sampling technique (**SI Appendix, Fig. S1A**). Wild-type GLIC and its mutants have been reconstituted in a mixture of POPE/POPG. Protein-lipid films were dried atop the internal reflection element and immersed in buffered aqueous solution. Difference spectra were calculated between sample spectra measured at various low pH values down to pH $\sim$ 2.0 and a reference spectrum measured at pH = 7.0. Peak positions of the bands in the FTIR spectra of the wild-type and the E35A mutant (**Fig. 2A-B**) are almost identical, with differences smaller than 2 cm^{-1}. All observed bands could be assigned either to the protein (1718-22, 1655, 1630, 1573, 1540, 1520, 1400 cm^{-1}), to the lipids (1738, 1466, 1456 cm^{-1}) or to the buffer (1364, 1321, 1218 cm^{-1}) as described in **SI Appendix, Materials and Methods**. Among the protein bands, those at $\sim$1720 cm^{-1} (ν(C=O)), $\sim$1573 cm^{-1} ($\nu_{as}(COO^-)$), and 1400 cm^{-1} ($\nu_s(COO^-)$) are assigned to the carboxylic acid/carboxylate group

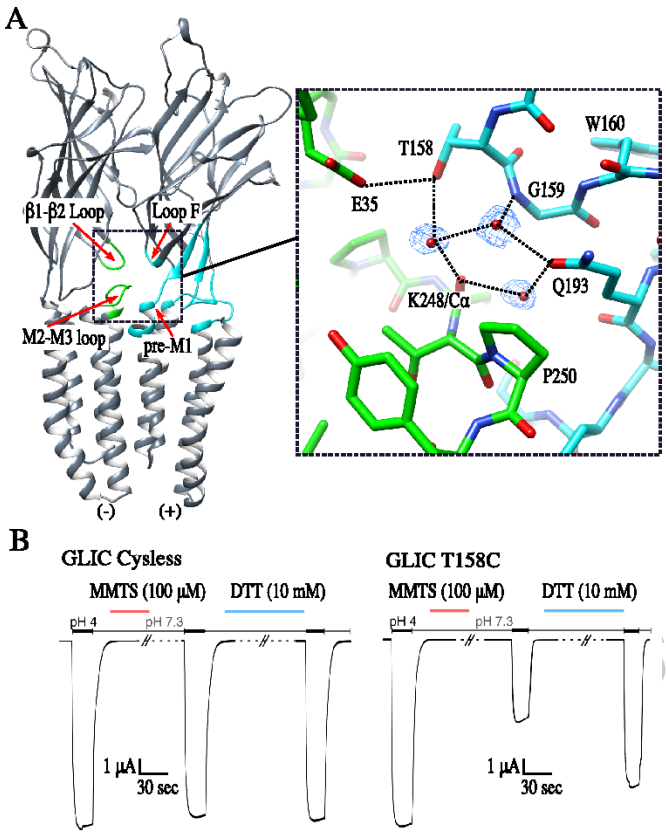

Fig. 3. Probing the immediate environment of E35. (**A**) Cartoon representation of the open form at 2.22 Å resolution for GLIC at pH 4. Only two subunits, viewed from the outside of the pentamer, are shown. The ECD and TMD interface loop regions are highlighted in green and blue. The inset shows structurally ordered water molecules at the ECD-TMD interface crevice. Water molecules are depicted as red spheres with blue mesh representation of 2mFo-DFc electron density map contoured at a level of 1 σ and overlaid. Surrounding residues are represented as sticks and labeled. Black dashed lines represent the hydrogen bonds network at the domain interface made of water molecules, Loop F, Q193 and the M2-M3 loop. (**B**) Effect of MMTS binding on the function of GLIC Cys-less and mutant T158C. The same recording protocol was used for all constructs (see **Materials and methods**).

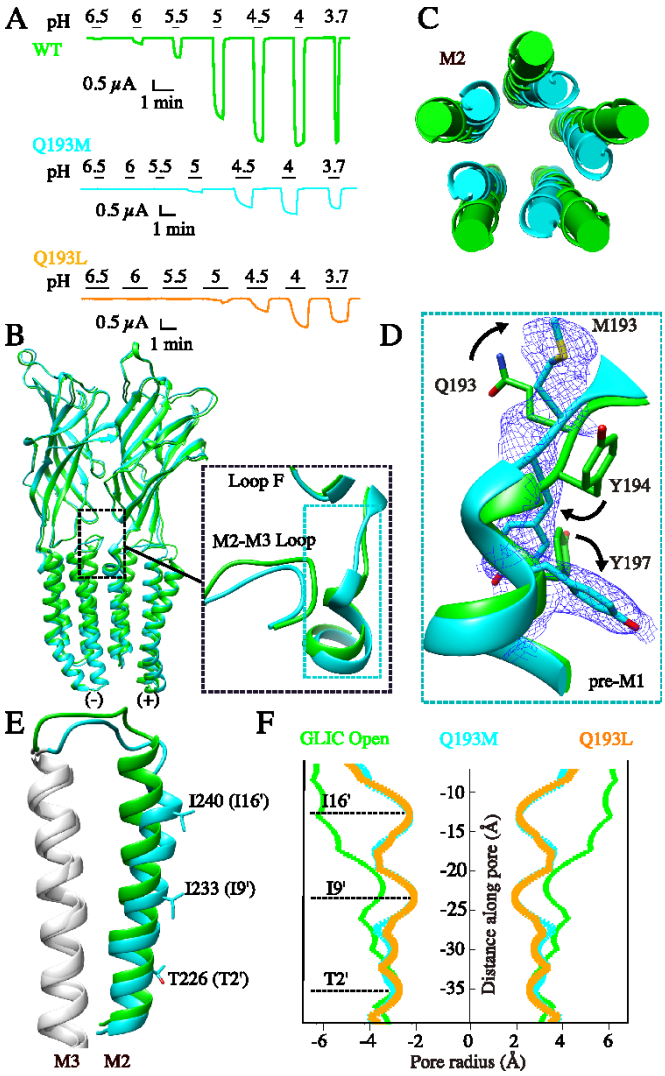

Fig. 4. Characterization of GLIC Q193M and Q193L mutations. (**A**) Proton-elicited currents from GLIC wild-type (green), Q193M (cyan) and Q193L (orange). (**B**) Structural superimposition of the GLIC Q193M (cyan) with the open form of wild-type GLIC (green). Only two subunits are shown viewed from the outside of the pentamer. Both structures are aligned using the whole pentamer. Inset shows an enlarged view of the pre-M1 region and of the M2-M3 loop reorganization. (**C**) Top view of the conformational change of M2 helices. (**D**). Conformational rearrangement of the pre-M1 region. The electron density of the 2mFo-DFc map around Q193M (blue) is contoured at the level of 1σ. (**E**) Side view of the conformational change of M2 helix, M2-M3 loop and M3 helix from one subunit. (**F**) Pore-radius profile for GLIC WT open (green), Q193M (cyan), Q193L (orange). The constriction sites in the Locally-Closed conformation from M2 helix are labeled and are shown as sticks in (**E**).

of Asp or Glu residues. An increase in the intensity of the ν(C=O) band due to the carboxylic acid (1720 cm^{-1}) is observed at lower pH due its protonation, along with the decrease of the intensity of $\nu_{as}(COO^-)$ and $\nu_s(COO^-)$ bands. Since the intensities of these bands indicate the extent of the protonation state of Asp and Glu residues in the protein, a plot of the intensity of these peaks as a function of pH provides a titration curve for the carboxyl groups. We note that a definite determination of peak positions and absolute intensities of ν(C=O) and $\nu_{as}(COO^-)$ are difficult to obtain as these bands closely overlap with lipid ester band at 1738 cm^{-1} and amide II band at 1540 cm^{-1}, respectively. Therefore, we used the $\nu_s(COO^-)$ band at 1400 cm^{-1} as a marker for the intensity analysis of carboxylic group, as it is sufficiently isolated from other bands (**Fig. 2A-B and SI Appendix, S1B-E**).

The normalized peak heights at 1400 cm^{-1} for the wild-type (black cross) and E35A mutant of GLIC (red dots) are shown in **Fig. 2C**. The intensities are normalized to be zero at pH = 7.0 and -1 at pH 2.0 for the wild-type GLIC receptor. These plots provide a titration curve of all Glu and Asp residues in GLIC. Since each GLIC subunit contains 16 Glu and 18 Asp residues, the overall titration curve displays a broad sigmoidal shape in a wide range of pH values due to the overlap of the individual titration curves from each residue. Notably, the pH titration curve from E35A mutant shows significant deviations from that of the wild-type receptor (**Fig. 2C-D**). Note that individual features of these titration curves are highly reproducible in a set of three independent experiments (**SI Appendix, Fig. S4**).

The differences in the pH titration curves become clear when the trace from the wild-type is subtracted from each of the mutant's trace. In a first approximation, one can show that the difference between the titration curves of the mutant and the wild-type represents the titration of the individual group that has been replaced by an alanine. The deviation of the traces is in the range of 2-7 % of the total intensity (**Fig. 2D**). Deviations in curves from the wild-type receptor between two different experiments do not exceed the range of ± 1%. Therefore, we only

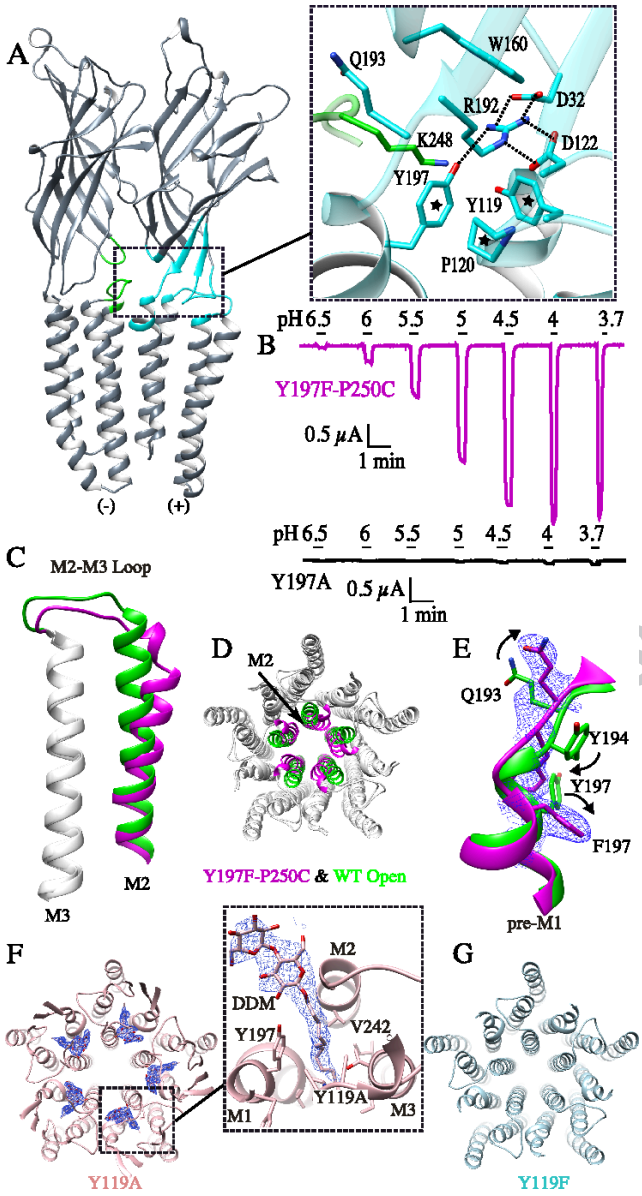

Fig. 5. The two electrostatic triads at the ECD-TMD interface governing channel gating. (A) Side view of two subunits of GLIC viewed from the outside of the pentamer. Inset shows a zoomed-in view of the inter-residue electrostatic network at the ECD-TMD interface. The salt bridges formed between R192, D122 and D32 are shown in dashed lines. Hydrophobic stacking interactions between residue Y197, P120, Y119 (Pro-Loop) are also highlighted by a star. The interaction between the primary electrostatic triad and the secondary electrostatic triad through Y197 (pre-M1) and R192 is shown in dashed lines. (**B**) Proton-elicited currents of GLIC Y197F and Y197A.(**C**) Conformational change of Y197F mutant structure (purple) in the M2 helix and the M2-M3 loop compared to the GLIC wild-type (green). (**D**) Top view of the TMD. (**E**) Conformational rearrangement of the pre-M1 region. The electron density 2mFo-DFc map of the Y197F mutant structure (blue mesh) is contoured at the level of 1σ. (**F**) Top view of the structure of Y119A in the TMD region. The detergent molecules inserted into the intra-subunit cavity are shown as sticks with a blue mesh representation of the 2Fo-Fc electron density map in its vicinity contoured at 1σ and overlaid. The inset zooms in on the zone of interaction of a detergent molecule with residues bordering the intra-subunit cavity. (**G**) Top view of the structure of Y119F in the TMD region.

consider mutants whose titration curves exhibit deviations > 2 %, as seen in the E35A and E181A variants. The other variants, E26A, E75A, E177A, and E104A, are below this criterion, thus we do not attempt to derive a pKa value for these groups (**Fig. 2D**). Experimental pKa values of E35 and E181 residues were determined to be 5.8 and 5.5, respectively, through fits to the Henderson-Hasselbalch equation (continuous lines in **Fig. 2D**).

We note that the trace of E35A (**Fig. 2D**) exhibits a sigmoidal shape, as expected for a canonical pH titration involving one proton. The abrupt decrease observed from pH 4.2 to 3.0 is not caused by an artifact caused by the instability of the lipid bilayer, as shown by the difference spectrum of the E243G mutant, which has a normal titration curve that is flat from pH 2.5 to 4 (**SI Appendix, Notes**). Rather, the decrease of the signal at pH < 4.2 can be explained by the change in pKa of one of the protonatable groups accessible to the solvent, induced by the mutation itself (**SI Appendix, Notes**). This adds a negative "bell-shaped curve" centered at around pH 3.8-4.2, on top of the regular pH-induced titration curve. Theory predicts that the pK_a^{eff} of E181 should be equal to $pK_a^{(c)}$–log K_D, which directly leads to an estimate of $K_D = 20$, where K_D is the equilibrium constant between the open and closed forms at pH 7 (**SI Appendix, Notes Eq. 14**). To our knowledge, this is the first time that this quantity, which is crucial in the allosteric model, is experimentally determined.

Probing residues around E35 by site-directed mutagenesis

Among the potential proton-sensing residues (pink zone in **Figure 1C**), E35 stands out as the only one whose individual pKa could be precisely measured with a well-defined transition curve by FT-IR, and its pKa value is indeed close to the pH_{50} determined by electrophysiology. Because E35 is not located at or close to the expected agonist-binding site of the pLGIC family, delineated by Loop C and Loop B, we performed a systematic study of its immediate environment by mutagenesis.

Exploring the role of Loop F by mutation and chemical labeling

Examination of the structure of GLIC indicates that E35 establishes a polar interaction with T158 from Loop F (**Fig. 3A inset**). To determine whether this interaction belongs to a network of interactions important for the global allosteric transition involved in gating, we probed this residue as well as those immediately adjacent in Loop F (G159, W160) by site-directed mutagenesis. Each position was mutated to a cysteine in order to perform further analysis through chemical labeling, and the impact of these mutations on the function of the corresponding residue was measured by electrophysiology. The Cys-less mutant of GLIC (C27S) has the same properties as the wild-type GLIC and is unaffected by treatment with MMTS (*S*-Methylmethanethiosulfonate), a reagent that blocks the side chain of cysteine and converts it into –S-S-CH_3 group, or with DTT (Dithiothreitol), that reduces S-S bonds. Cysteine replacement of T158 does not affect the function of the receptor. However, when T158C mutant is labeled with MMTS, the current is decreased by 50%. This phenotype can be reversed by reducing and removing the MMTS labeling (**Fig. 3B**). G159C mutation totally abolishes the pH-induced currents and generates a nonfunctional receptor; this is also the case of the W160C mutant (**SI Appendix, Table S2**). Expression tests in oocytes show that W160C is not expressed and G159C has a low expression level, but still detectable (**SI Appendix, Fig S11**), indicating that the two residues located in Loop F are not only functionally important but also structurally crucial for the receptor. Notably, the side chain of W160 is stacked above the strictly conserved residue R192 (**Fig. 5A**). We noted earlier that the TGW sequence in GLIC's Loop F is special, where it is usually [G]EW in cationic pLGICs[43] (**Fig. 6B**).

A water-mediated electrostatic network at the ECD-TMD interface stabilizes the open form structure

An open-form crystal structure of GLIC was determined at 2.22 Å resolution and has significantly better refinement statistics than the previously known 2.4 Å structure (**SI Appendix, Table S3**), which allows a more detailed study of the bound water molecules. A close analysis of this high-resolution model uncovers

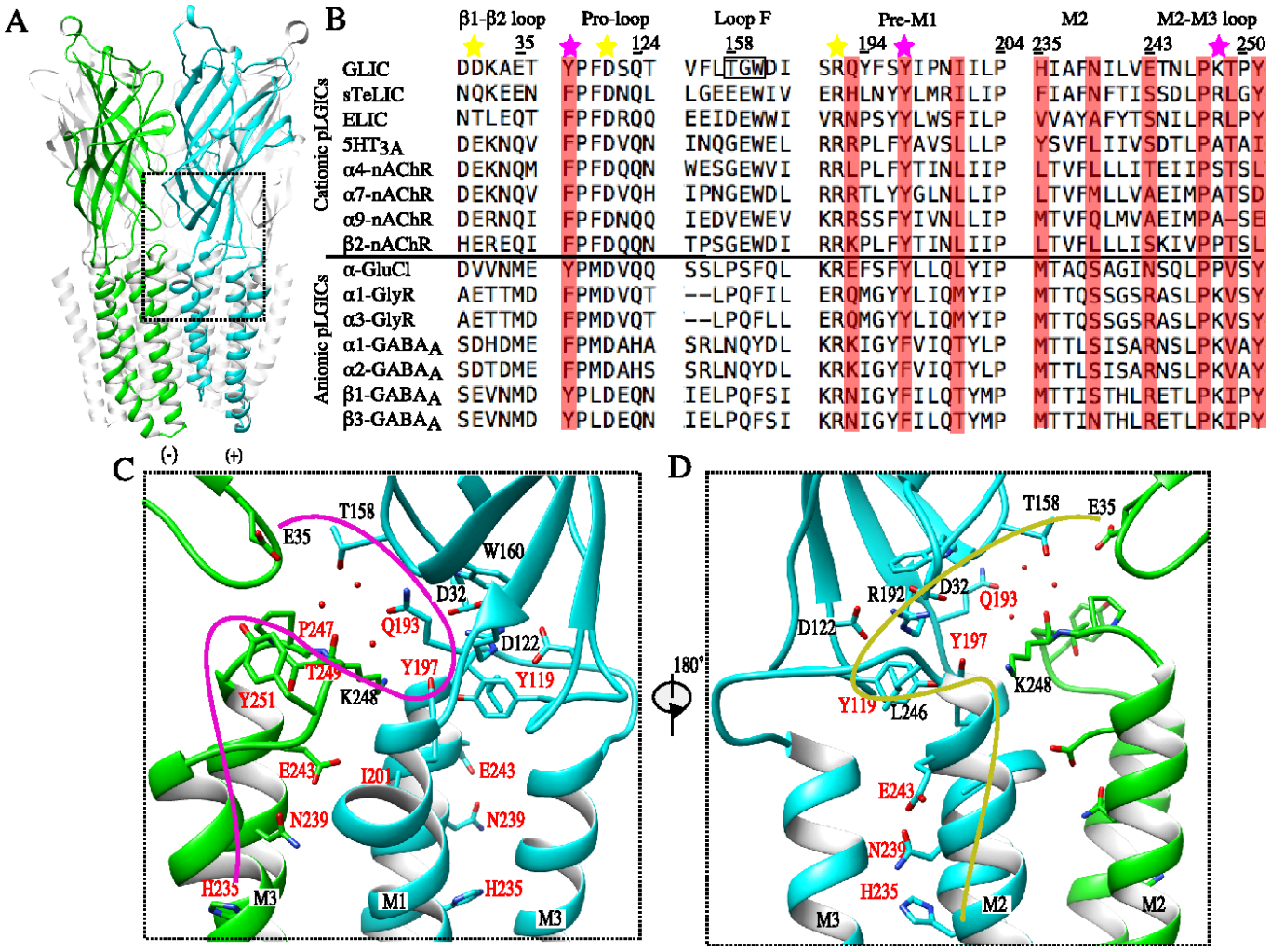

Fig. 6. Figure 6 Two stabilization networks are used in GLIC to maintain the channel open. (**A**) View of the GLIC wild-type open-form structure. Two adjacent subunits are highlighted. (**B**) Multiple-sequence alignment of GLIC and its homologs in a limited set of regions to highlight the positions in GLIC (colored in red) whose mutation traps GLIC in Locally-Closed conformation. The alignment contains GLIC (*G. violaceus*) and ELIC (*E. chrysanthemi),* sTeLIC (symbiont of the worm *Tevnia*), GluCl (a glutamate-gated chloride ion channel from *C. elegans*) and α1-GlyR (the glycine receptor α1 subunit from *Zebrafish),* $5HT_{3A}$ (the serotonin receptor from mouse). The remaining sequences arerepresentatives for human pLGICs. Numbering refers to the GLIC protein sequence. The yellow stars indicate the residues forming the primary electrostatic triad and the purple stars indicate residues involved in the secondary electrostatic triad. The TGW motif in GLIC is boxed. (**C-D**) Two branches of a continuous network originating from E35 that reach, independently, the middle transmembrane region (H235) of two adjacent subunits. The proton-sensor E35 and key residues responsible for channel activation are shown as sticks. (**C**) View from outside the pentamer with the first network shown as a purple line, across subunits. (**D**) View from inside the pentamer showing the second network involving the hydrophobic cluster as an orange line, within the same subunit.

the existence of an elaborate hydrogen bond network at the ECD-TMD interface. The side chain of Q193 interacts with the backbone amide nitrogen atom of G159 from loop F, as well as with the carbonyl oxygen atom of K248 from the M2-M3 loop of the adjacent subunit through hydrogen bonds mediated by water molecules. This hydrogen bond network at the ECD-TMD interface extends to residue T158 of Loop F, which is in turn interacting with E35 (**Fig. 3A and inset**).

Probing the interfacial hydrophilic crevice centered on Q193

First, Q193 has been replaced by a hydrophobic residue, either methionine or leucine. Electrophysiology experiments show that both mutants exhibit a loss-of-function phenotype with pH_{50} = 4.53 ± 0.02 and pH_{50} = 4.48 ± 0.05 compared to that of wild-type pH_{50} = 5.10 ± 0.20 (**Fig. 4A** and **SI Appendix, Table S2**). We solved the crystal structures of Q193M and Q193L at pH 4 with 2.95 Å and 3.39 Å resolution. Unexpectedly, both mutants adopt the conformation previously described as LC1 in the "Locally Closed"[16] or "fully-liganded closed-channel" forms[17]. When superimposed to GLIC H235F, the very first LC1 form of GLIC (PDB ID: 3TLC)[16], the Q193M and Q193L mutants show a root mean square deviation (RMSD) of 0.61 Å and 0.59 Å, respectively. All five M2 α-helices are kinked at the level of the I9' position. The upper portion of M2 helices tilts and rotates clockwise around the five-fold symmetry axis along the ion channel pore, and consequently narrow the ion permeation pathway, generating a nonconductive ion channel (**Fig. 4C** and **Fig. 4E-F**). Compared to the wild-type open-form structure, the side chains of M193/L193 rotate by 90° and do not protrude into the interfacial crevice any more (**Fig. 4D**). Thus, breaking the hydrogen bond network by replacing Q193 with hydrophobic residues hinders gating and destabilizes the open form.

We further probed the ECD-TMD interfacial hydrogen bond network by replacing Q193 with a cysteine to introduce a shorter and less polar side chain. The phenotype of Q193C was almost identical to that of the wild-type (**SI Appendix, Table S2**). Consistently, the 2.58 Å resolution structure of Q193C adopts the open

Table 1. Structural mapping of the mutations that trap GLIC in a Locally Closed conformation

Variant	Location	Conformation (Phenotype)	Note
Q193C+MMTS	Pre-M1	LC1 (Loss of function)	This study
Q193L	Pre-M1	LC1 (Loss of function)	This study
Q193M	Pre-M1	LC1 (Loss of function)	This study
Y197F-P250C	Pre-M1	LC1 (Wild type phenotype)	This study
I201W- E243C	Pre-M1	LC2 (Nonfunctional)	This study
H235F (H11'F)	Upper M2	LC1 (Nonfunctional)	PDB ID 3TLT
H235Q (H11'Q)	Upper M2	LC (Loss of function)	PDB ID 5NJY
N239C (N15'C)	Upper M2	LC (Loss of function)	PDB ID 5NKJ
E243G (E19'G)	Upper M2	LC2 (Nonfunctional)	This study
E243P (E19'P)	Upper M2	LC2 (Nonfunctional)	PDB ID 3TLS
P247G (P23'G)	M2-M3 loop	LC2 (Loss of function)	PDB ID 5HEG
T249A (T25'A)	M2-M3 loop	LC1 (Nonfunctional)	PDB ID 4LMJ
Y251A (Y27'A)	M2-M3 loop	LC1 (Nonfunctional)	PDB ID 4MLM
Wild type-10*His	C-terminal 10*His	LC and Open Co-exist	PDB ID 4NPP
K33C-T20'C	Loop2 and M2-M3 loop	LC1 (Nonfunctional)	PDB ID: 3UU3
K33C-N21'C	Loop2 and M2-M3 loop	LC2 (Nonfunctional)	PDB ID 3TLW
K33C-L22'C	Loop2 and M2-M3 loop	LC3 (Loss of function)	PDB ID 3TLV
K33C-K24'C	Loop 2 and M2-M3 loop	LC1 (Nonfunctional)	PDB ID 3TLU

conformation at pH 4 (**SI Appendix, Fig. S7A**). The structure shows a water molecule in the interfacial crevice region that connects the thiol group of C193 to the nitrogen atom of G159 and to the nitrogen atom of P250 of the neighboring subunit (**SI Appendix, Fig. S7B inset**). The resulting hydrogen bond network was probed by additional experiments to confirm its putative role in maintaining the channel open. First, Labelling Q193C with MMTS leads to a 75% current decrease, which is reversed by DTT reduction. Thus, breaking the new interfacial hydrogen bond network destabilizes the open form of the channel. Next, the co-crystallized structure of Q193C with MMTS shows a conformation similar to that Q193M (**SI Appendix, Fig. S7C-D**) and the 2mFo – DFc map shows density for the MMTS covalently linked molecule (**SI Appendix, Fig. S5E-F**). In addition, we tried to enhance the interaction of Q193C with the M2-M3 loop by introducing a second cysteine residue (P250C), in a position such that it could form a disulfide bridge with Q193C. As predicted, this double mutation shows a strong 'gain-of-function' phenotype. In oocytes expressing GLIC Q193C-P250C receptors, the recording shows an apparent leak of current at pH 7 that can be blocked by picrotoxin, an open channel blocker (**SI Appendix, Fig. S8C**), and abolished by treatment with DTT. All those evidences point to the key role of the residue Q193 located at pre-M1 region in coupling proton binding to channel opening.

Preceding Q193, residue R192 interacts with two negatively charged residues: D122 and D32. This triplet forms a bifurcated salt bridge that is conserved among pLGIC receptors and has been shown to be functionally important for channel activation[18], [44]. Furthermore, the 2.22 Å structure clearly shows that the water molecule network linking E35 to Q193 can be further extended to Y197 and R192 (**SI Appendix, Fig. S5**). While the apolar atoms of the side chain of the strictly conserved P120 (Pro-loop) interact with those of Y119 and Y197 through hydrophobic interactions, the hydroxyl group of Y197 interacts with the side chain of R192 (**SI Appendix, Fig. 5A inset**). Therefore, residues Y197-K248-Y119 form a secondary electrostatic triad that interacts with the primary one in the open form.

Probing the tyrosine residues from the secondary electrostatic triad at the ECD-TMD interface

The FD-DH method predicts that the two tyrosine from the secondary electrostatic triad have a highly ΔpKa value (**SI Appendix, Fig. S9**). At the structural level, Y197 stands out as undergoing a switch of its side chain from an "inward" position to an "outward" position when switching from the LC1 form to the open-form. During this re-arrangement of the pre-M1 region, Y194, which points toward the lipid bilayer in the open form, also flips its orientation by almost 180° and becomes buried inside the inter-subunit cavity (**Fig. 4D**). This breaks the interaction of Y197 with R192. To test whether both the hydroxyl and aromatic groups are required for proton-elicited channel currents, we mutated Y197 to phenylalanine and alanine separately.

The pH 4 crystal structure of Y197F mutant is identical to that of Q193M/Q193L, with the side chains of Y194 and Y197F adopting the same conformations as in the model of Q193M/Q193L (**Fig. 5C-E**). However, on the functional level, Y197F does not show any decrease in proton sensitivity, with a pH_{50} identical to the wild-type GLIC (**Fig. 5B** and **SI Appendix, Table S2**). This suggests that even though the activation barrier between the Locally Closed form and the open form is increased, it can still be crossed to lead to the open conformation of the channel in solution, contrary to what is seen in Q193M/Q193L. Since the aromatic ring of Y197 interacts with P120 (Pro-loop), Y119 (Pro-loop) and L246 (M2-M3 loop) through hydrophobic or stacking interactions, we replaced Y197 by an alanine (Y197A) to disrupt the interaction between Y197 and R192, and to reduce the hydrophobic stacking between both the Pro-loop and the M2-M3 loop. The Y197A mutation completely abolishes the function of the channel. (**Fig. 5B** and **SI Appendix, Table S2**). We could only get a 7Å data set from crystals of Y197A, but we could nevertheless assess that Y197A mutation traps the receptor in the LC form (**SI Appendix, Fig. S10**). Hence, our data indicate that the aromatic residue Y197 plays a crucial role in the coupling of proton binding to channel gating.

Y119 is predicted to also have a large ΔpKa value (ΔpKa = 2.7) (**SI Appendix, Fig. S9B**). The crystal structure of Y119F displays an open conformation, which is in line with functional recordings that show a wild-type phenotype. Furthermore, the 2.8 Å crystal structure of Y119A mutant, that generates a non-functional receptor[18], adopts an open conformation (**Fig. 5F-G**), but with additional strong and continuous electron density in the Fourier mFo-DFc difference map near the mutation site (average peak height at 7.5 σ), indicative of the presence of a bound molecule that we interpreted as a detergent molecule (DDM) in each of the subunit. DDM, that we used during the purification and crystallization of the receptor, is positioned in such a way that its sugar moiety is exposed to the ECD lumen and its hydrophobic tail inserts into the cavity vacated by the removal of the phenylalanine side chain (**Fig. 5F inset**). Therefore, we propose that in this case the hydrophobic tail of DDM fulfills the role of the aromatic ring of Y119 to artificially maintain the channel open. Interestingly, this cavity largely overlaps with the

site that has been shown to contribute to the binding of propofol and desflurane[22].

We also explored the role of K248, which is involved in the secondary electrostatic triad, by solving the structures of K248C and K248A mutants. Their structures are wild-type-like at pH 4 (**SI Appendix, Table S3**): in K248C, the cysteine side-chain is still able to make a hydrogen bond with Y197 and for K248A, N245 changes rotamer to make one more hydrogen bond with Y197, indicating a compensatory role of this site.

Mutations that trap the channel in the LC form reveal two different networks that stabilize the open form of the channel down to H235

One interfacial hydrophilic network connects E35 to the entrance of the channel pore (E243) and further down to H235

One of the new results of the FD-DH calculations is the existence of a triad of strong electrostatic interactions involving Y119-Y197 and K248(+) (adjacent subunit) that extends the R192-D122-D32 well known triad. Y197 can actually interact with two different M2-M3 loops, one from the same subunit (through L246) via the Pro-Loop, and one from the adjacent subunit (through K248) (**Fig. 5A inset**). E243 marks the entrance of the channel. Strikingly, its side chain can adopt two different conformations in the open form [32]. However, electrophysiology recordings show that E243C has almost the same pH_{50} value as the wild-type[19]. Consistent with electrophysiology results, E243C structure shows no distinguishable difference with the open form of GLIC (RSMD = 0.215 Å) (**SI Appendix, Fig. S12A**). To further probe the site of E243, the substitution E243G was generated: it results in a closed channel, similar to E243P, whose structure was previously reported to be in the Locally Closed (LC2) conformation (**SI Appendix, Fig. S12C**). Collectively, our data suggest that E243 is probably not a key residue for proton sensing; rather, it is crucial for maintaining the stability of the upper part of M2 helix during the channel opening. Strikingly, if one goes down the M2 helix starting at E243 by steps of 4 residues, on the same side of the helix, one finds N239 and H235 whose mutation stabilizes in both cases the LC form in the crystal[45]. In conclusion, by connecting the dots between positions whose mutations trap the receptor in an LC-form, the network Y197-K248-E243-N239-H235 further extends the network that originates from E35, Q193 and Y197, going deeply to the TMD of the adjacent subunit (**Fig. 6C**).

A different interfacial network that involves hydrophobic sidechains connects E35 to the pre-M1 and to a TMD intra-subunit cavity known to bind general anesthetics (GAs)

The hydrophobic network originating from the Y197-P120-Y119 interactions reaches out to L246 from the M2-M3 loop of the same subunit to build up a second ramification of the network connecting mutants stabilizing an agonist-bound but inactive form, in such a way that it completely encircles the ECD-TMD interface of the pentamer (**Fig. 6D**). Indeed, it contains residues close to L246 that have been mutated in previous studies and found to lead to the LC-form as well, namely P247G[18] and Y249 and T251[17].

Upon channel opening, the tightly packed bundle of five M2 helices detach from each other and move closer to M3 helices. This reshapes a cavity located behind the M2 helix and beneath the residues Y197-P120-Y119, that is essential for general anesthetics binding[22]. Structure analysis predicted that the mutation I201W (Pre-M1), introducing a bulky amino acid in that cavity, would block the M2 helices movement. Indeed, the mutant I201W generates a nonfunctional receptor[19]. The crystal structure of I201W shows a LC conformation, the same as that of E243G (**SI Appendix, Fig. S12B** and **SI Appendix, Fig. S13**). In the open form of GLIC, the side chain of I201 contacts the hydrophobic residue F238 (F14'), L241 (L17') and V242 (V18') within the M2 helix of the same subunit (**SI Appendix, Fig. S12E**). The new bulky residue in I201W occupies this cavity and hinders the movement of the upper part of the M2 helix. Hence, this tightly packed hydrophobic network is also important for GLIC function and its modulation by pharmacological reagents.

Discussion

The structures of pairs of open and closed forms of the ion channel, in the case of GLIC[13], [15], [20], GluCl[5], [6] and GlyR[10] open the way to an understanding of the conformational transitions that take place during gating in pLGICs. Previous work has focused on normal mode analysis and coarse-grained methods to predict possible transition pathways from pairs of structures and simplified models of the proteins based on a mixture of elastic network models[20], [46]. In addition, experimental studies such as the measurement of the coupling phi-values using site-directed mutagenesis and patch clamp electrophysiology can provide detailed models of the sequence of events leading to the opening of the channel[47], [48]. Also, time-resolved fluorescence quenching experiments can give information on the conformational transitions of the receptors in the millisecond scale[19]. Fully atomistic molecular dynamics studies have also been used on the TMD alone[49] or on the full GluCl receptor, either for the gating or un-gating transition[50], [51]. Recently, MD simulations were used to generate possible transition pathways for the gating in GLIC through the string method [52]. For pH-gating, however, there is an additional difficulty in assigning the protonation state of all Asp, Glu and His residues in the two end states. Presently, it is not known with certainty which of these residues are protonated concomitantly with the conformational transition, and current MD experiments do not allow the (reversible) change of protonation state of titratable residues during simulations of such large systems. Therefore, more experimental studies are needed to help resolve this question.

Our studies do not contain any temporal information; however, they reveal a crucial proton-sensing residue, from which we progressively build up and extend a network of interactions that are essential for the stabilization of the open form. In that regard, we do not support the search for an "allosteric network" that would propagate information from the orthosteric site to the channel itself[53] and confine ourselves to the strict theory of allostery, which postulates a global transition between two forms of the same macromolecule (resting and active). Here, we could determine the K_D between the two forms in the absence of the ligand, which shows the presence of 5% of the bound form without any ligand. Strikingly, residues whose mutations perturb this equilibrium form a network of spatially connected residues. This network potentially provides a framework for the interpretation of a large body of experimental data.

The proton-sensing residue is located opposite to Loop F and may bypass the classical agonist-binding site

One of the major questions in the GLIC gating transition is to identify its proton sensor(s). It has been known for some time that several regions at the ECD-TMD interface are crucial for the gating transition [18]. However, the exact role of all 34 carboxylate residues in the conformational change that occurs upon dropping the extracellular pH, has remained elusive up to now. To identify the proton-sensing residues responsible for the gating transition, systematic site-directed mutagenesis of all Asp or Glu residues was undertaken, followed by both functional and structural characterization of the mutants[40]. These studies have an inherent limitation in that only the *global* pH_{50} of the transition is measured, for all the remaining Asp and Glu [54]. Here we go further by using pH-induced FT-IR spectroscopy and difference spectra to *individually* titrate a list of candidate Asp/Glu residues selected computationally by detailed electrostatic calculations.

E35 stands out as the main proton-sensor. It is located at the end of the β1-β2 loop and interacts with Loop F of the

next subunit through residue T158. Experiments involving the chemical labeling of T158C with MMTS showed the importance of this residue for channel opening. This is similar to experiments performed on the same position in ELIC, which also lead to the conclusion that this position is very important for the gating transition[27]. Loop F has been shown to be responsible for the inhibition of some pLGICs by divalent ions, such as Ca^{++} ions for ELIC and for nAChR, and Zn^{++} for GABA-R [53]–[55]. Recently, Ulens and coll. showed that one should distinguish between the upper Loop F binding site, occupied by bromoform in ELIC and Xenon in GLIC, and the lower Loop F binding site, occupied by chlorpromazine[58]. Strikingly, examination of the GLIC structure strongly suggests that mutation to W160 in Loop F will affect the stability of the R192-D122-D32 salt bridge due to the stacking interaction between the side chains of R192 and W160. Furthermore, compared with the resting state of GLIC, a marked backbone shift of Loop F is observed in the open state of GLIC[20]. Also, EPR studies showed that big movements of Loop F occur during activation in GLIC[30], [59].

In the eukaryotic pLGIC family, the gating equilibrium is governed by neurotransmitter binding to the LoopC/Loop B region[14]. The key proton sensor E35 is not close to Loop C and Loop B. The backbone of Loop C also shifts markedly between the open and closed states. We propose that proton-gating in GLIC bypasses the "classical" orthosteric site and that, instead, a consequence of the "bidirectional effect" in allostery (or "reciprocity principle" [60]) is observed, whereby the modification of Loop F would be concomitant with (but not driven by) a rearrangement of Loop C similar to what is observed in a pLGIC gated by a neurotransmitter.

Mapping residues stabilizing the Locally-Closed form informs on the transition pathway

The crystal structures of the open and LC states of GLIC are both captured at pH 4. Because it is fully protonated and has a closed pore, the LC-form represents an "agonist-bound closed form" of GLIC; it was found in three variant forms termed LC1, LC2 and LC3[16]. In the LC2 conformation (E243G and I201W in this study), the deformation of the end turn of M2 helices stabilizes the closed pore but the M2-M3 loop conformation is unaltered. In the LC1 conformation (Q193M/L, Q193C+MMTS and Y197F in this study), the mutation in the pre-M1 region presumably impairs the coupling of the ECD and TMD, the M2 helix end turn is destabilized and the M2-M3 loop conformation is changed. In the LC3 conformation the M2 helix is further destabilized at its C-terminus. LC2 has been suggested to represent a pre-activation form, as inferred by detailed kinetics studies of the transition[19]. Recently, more mutations further down on the same face of the M2 helix at positions N239 and H235, were also shown to lead to the stabilization of the LC1 form[45]. Here we go further by producing mutants in the pre-M1 region that also stabilize the LC1 form at positions 193 and 197 (**Table 1**), extending the network of positions where a mutation can change the equilibrium between the two forms and providing a link with the proton-sensing residue E35. The open and LC1 forms actually co-exist in the same crystal at pH 4[20]. This indicates a low energy barrier between these two conformations such that single-point mutations can modify it with a clear readout (**SI Appendix, Fig. S14D-E**). This unique property enables us to map the residues that are important for the stabilization of the open form.

Structure-based activation model with two alternative stabilization networks originating from the same ECD subunit interface and plunging into the TMD

If we simply connect together those positions where mutants adopt any of the LC-forms, we can propose a model for the coupling between proton binding and channel gating. First the ECD undergoes a conformational change stabilized by an increase of the proton concentration, probably starting with the protonation of E35 (pKa = 5.8) when the pH is lowered from 7 to 4. This would be associated with several changes in the ECD-TMD interface: i) A change in loop F (T158, G159, W160), also affecting R192 through its hydrophobic stacking interactions with the side-chain of W160, ii) The local rearrangement of the β1-β2 loop (including D32), tightening the D122-R192-D32 triple salt bridge, iii) The pre-M1 region (Q193) through the described water-mediated hydrogen bond network at the ECD-TMD interface, again affecting R192 directly. The R192 primary triad is also linked in the open form of GLIC to a secondary electrostatic triad involving Y197 (pre-M1), Y119 (Pro-Loop) and the M2-M3 loop (K248) of the adjacent subunit (**SI Appendix, Fig. S14A-C**).

On one side of Y197, the rearrangement of the M2-M3 loop through L246 is accompanied by a counter-clockwise movement of the upper portion of M2 helices that generates a conductive channel pore; this movement also reshapes the TMD intra-subunit cavity probed by general anesthetics [22]. Together with other data on the M2-M3 loop[16], this supports the idea that the coupling between the pre-M1 region, Pro-loop and M2-M3 loop is mediated, at least partly, by a hydrophobic cluster within each subunit that stabilizes the open form of the channel (**Fig. 6D**). On the other side of Y197, another electrostatic network involves Y119, K248 of the next subunit as well as E243. Strikingly, H235 and N239 have been shown to also be a binding site for several general anesthetics that, in some mutants of GLIC, can switch the receptor back and forth from the open to the closed-forms, when they bind[45] (**Fig. 6C**). Altogether, the network of residues stabilizing the LC forms both percolate to the center of the TMD region and circulate between subunits. Residues involved in the stabilization networks described here were also shown to strongly affect the activation energy between the open and closed forms of eukaryotic pLGICs[44]. Thus, we anticipate that the same activation model should be a general feature of pLGICs.

Our findings underline the importance of electrostatics in understanding the conformational transitions of pLGICs. First, the binding of the charged neurotransmitter (a cation in 5HT3 or ACh, or a zwitterion in GABA or Gly) changes the interface between ECDs, which is known to be highly deformable[61], immediately followed by solvent relaxation and adaptation of the surface charges at the lipid-water interface. In this respect, the presence of two separate electrostatic triads at the ECD-TMD interface is perhaps not so surprising. Second, the opening of the channel also leads to a major change of the electrostatic energy, if one considers transmembrane helices as simple macro-dipoles. Finally, the permeation of ions drastically changes the electrostatic energy by setting to zero the local transmembrane potential, thus leading to another conformational transition of the receptor, this time to the desensitized form, probably accompanied by the relaxation of the lipid-TMD interactions. We expect that MD simulations explicitly taking into account the difference of ionic concentrations on each side of the membrane will give further insight into the conformational transitions of members of the pLGIC family.

Materials and Methods

GLIC was expressed and purified crystallized according to the protocol described in ref (13). The electrophysiology experiments were performed on GLIC expressed in *Xenopus laevis* oocytes. FT-IR experiments were carried out by reconstitution of GLIC and its variants in POPE/POPG lipids. Full materials and methods are available in Supplementary files.

Acknowledgements

We would like to thank the staff at crystallization platform of Institut Pasteur. We thank the staff at ESRF and Synchrotron-Soleil for excellent beamline facilities. We thank Marie Prevost and Solène Lefebvre for assistance during the manuscript revisions. ZFK was supported by Grant Pentagate ANR 13 BSV 8. Haidai Hu was sponsored by CSC and Institut Pasteur.

[1] P.-J. Corringer, F. Poitevin, M. S. Prevost, L. Sauguet, M. Delarue, and J.-P. Changeux, 'Structure and Pharmacology of Pentameric Receptor Channels: From Bacteria to Brain', *Structure*, vol. 20, no. 6, pp. 941–956, Jun. 2012.

[2] M. Jaiteh, A. Taly, and J. Hénin, 'Evolution of Pentameric Ligand-Gated Ion Channels: Pro-Loop Receptors', *PLOS ONE*, vol. 11, no. 3, p. e0151934, Mar. 2016.

[3] W. Y. Lee, C. Free, and S. M. Sine, 'Binding to gating transduction in nicotinic receptors: Cys-loop energetically couples to pre-M1 and M2-M3 regions', *J. Neurosci. Off. J. Soc. Neurosci.*, vol. 29, no. 10, pp. 3189–3199, Mar. 2009.

[4] L. Sauguet, A. Shahsavar, and M. Delarue, 'Crystallographic studies of pharmacological sites in pentameric ligand-gated ion channels', *Biochim. Biophys. Acta*, vol. 1850, no. 3, pp. 511–523, Mar. 2015.

[5] T. Althoff, R. E. Hibbs, S. Banerjee, and E. Gouaux, 'X-ray structures of GluCl in apo states reveal a gating mechanism of Cys-loop receptors', *Nature*, vol. 512, no. 7514, pp. 333–337, Aug. 2014.

[6] R. E. Hibbs and E. Gouaux, 'Principles of activation and permeation in an anion-selective Cys-loop receptor', *Nature*, vol. 474, no. 7349, pp. 54–60, Jun. 2011.

[7] P. S. Miller and A. R. Aricescu, 'Crystal structure of a human GABAA receptor', *Nature*, vol. 512, no. 7514, pp. 270–275, 2014.

[8] X. Huang, H. Chen, K. Michelsen, S. Schneider, and P. L. Shaffer, 'Crystal structure of human glycine receptor-α3 bound to antagonist strychnine', *Nature*, vol. 526, no. 7572, pp. 277–280, 2015.

[9] C. L. Morales-Perez, C. M. Noviello, and R. E. Hibbs, 'X-ray structure of the human α4β2 nicotinic receptor', *Nature*, vol. 538, no. 7625, pp. 411–415, 2016.

[10] J. Du, W. Lü, S. Wu, Y. Cheng, and E. Gouaux, 'Glycine receptor mechanism elucidated by electron cryo-microscopy', *Nature*, vol. 526, no. 7572, pp. 224–229, 2015.

[11] G. Hassaine *et al.*, 'X-ray structure of the mouse serotonin 5-HT3 receptor', *Nature*, vol. 512, no. 7514, pp. 276–281, 2014.

[12] R. J. C. Hilf and R. Dutzler, 'X-ray structure of a prokaryotic pentameric ligand-gated ion channel', *Nature*, vol. 452, no. 7185, pp. 375–379, Mar. 2008.

[13] N. Bocquet *et al.*, 'X-ray structure of a pentameric ligand-gated ion channel in an apparently open conformation', *Nature*, vol. 457, no. 7225, pp. 111–114, 2009.

[14] A. J. R. Plested, 'Structural mechanisms of activation and desensitization in neurotransmitter-gated ion channels', *Nat. Struct. Mol. Biol.*, vol. 23, no. 6, pp. 494–502, 2016.

[15] R. J. C. Hilf and R. Dutzler, 'Structure of a potentially open state of a proton-activated pentameric ligand-gated ion channel', *Nature*, vol. 457, no. 7225, pp. 115–118, Jan. 2009.

[16] M. S. Prevost *et al.*, 'A locally closed conformation of a bacterial pentameric proton-gated ion channel', *Nat. Struct. Mol. Biol.*, vol. 19, no. 6, pp. 642–649, May 2012.

[17] G. Gonzalez-Gutierrez, L. G. Cuello, S. K. Nair, and C. Grosman, 'Gating of the proton-gated ion channel from Gloeobacter violaceus at pH 4 as revealed by X-ray crystallography', *Proc. Natl. Acad. Sci. U. S. A.*, vol. 110, no. 46, pp. 18716–18721, Nov. 2013.

[18] C. Bertozzi, I. Zimmermann, S. Engeler, R. J. C. Hilf, and R. Dutzler, 'Signal Transduction at the Domain Interface of Prokaryotic Pentameric Ligand-Gated Ion Channels', *PLoS Biol.*, vol. 14, no. 3, p. e1002393, Mar. 2016.

[19] A. Menny *et al.*, 'Identification of a pre-active conformation of a pentameric channel receptor', *eLife*, vol. 6, Mar. 2017.

[20] L. Sauguet *et al.*, 'Crystal structures of a pentameric ligand-gated ion channel provide a mechanism for activation', *Proc. Natl. Acad. Sci. U. S. A.*, vol. 111, no. 3, pp. 966–971, Jan. 2014.

[21] S. Basak, N. Schmandt, Y. Gicheru, and S. Chakrapani, 'Crystal structure and dynamics of a lipid-induced potential desensitized-state of a pentameric ligand-gated channel', *eLife*, vol. 6, p. e23886, Mar. 2017.

[22] H. Nury *et al.*, 'X-ray structures of general anaesthetics bound to a pentameric ligand-gated ion channel', *Nature*, vol. 469, no. 7330, pp. 428–431, Jan. 2011.

[23] L. Sauguet *et al.*, 'Structural basis for potentiation by alcohols and anaesthetics in a ligand-gated ion channel', *Nat. Commun.*, vol. 4, p. ncomms2682, Apr. 2013.

[24] B. Laurent, S. Murail, A. Shahsavar, L. Sauguet, M. Delarue, and M. Baaden, 'Sites of Anesthetic Inhibitory Action on a Cationic Ligand-Gated Ion Channel', *Struct. Lond. Engl. 1993*, vol. 24, no. 4, pp. 595–605, Apr. 2016.

[25] R. J. Howard *et al.*, 'Structural basis for alcohol modulation of a pentameric ligand-gated ion channel', *Proc. Natl. Acad. Sci. U. S. A.*, vol. 108, no. 29, pp. 12149–12154, Jul. 2011.

[26] Z. Fourati *et al.*, 'Barbiturates Bind in the GLIC Ion Channel Pore and Cause Inhibition by Stabilizing a Closed State', *J. Biol. Chem.*, vol. 292, no. 5, pp. 1550–1558, Feb. 2017.

[27] M. Nys *et al.*, 'Allosteric binding site in a Cys-loop receptor ligand-binding domain unveiled in the crystal structure of ELIC in complex with chlorpromazine', *Proc. Natl. Acad. Sci.*, vol. 113, no. 43, pp. E6696–E6703, Oct. 2016.

[28] R. Spurny *et al.*, 'Pentameric ligand-gated ion channel ELIC is activated by GABA and modulated by benzodiazepines', *Proc. Natl. Acad. Sci.*, vol. 109, no. 44, pp. E3028–E3034, Oct. 2012.

[29] R. Spurny *et al.*, 'Multisite Binding of a General Anesthetic to the Prokaryotic Pentameric Erwinia chrysanthemi Ligand-gated Ion Channel (ELIC)', *J. Biol. Chem.*, vol. 288, no. 12, pp. 8355–8364, Mar. 2013.

[30] C. D. Dellisanti *et al.*, 'Site-Directed Spin Labeling Reveals Pentameric Ligand-Gated Ion Channel Gating Motions', *PLOS Biol.*, vol. 11, no. 11, p. e1001714, Nov. 2013.

[31] M. Gielen and P.-J. Corringer, 'The dual-gate model for pentameric ligand-gated ion channels activation and desensitization', *J. Physiol.*, Feb. 2018.

[32] L. Sauguet *et al.*, 'Structural basis for ion permeation mechanism in pentameric ligand-gated ion channels', *EMBO J.*, vol. 32, no. 5, pp. 728–741, Mar. 2013.

[33] M. Gielen, P. Thomas, and T. G. Smart, 'The desensitization gate of inhibitory Cys-loop receptors', *Nat. Commun.*, vol. 6, p. 6829, Apr. 2015.

[34] K. E. Mounsey, J. A. Dent, D. C. Holt, J. McCarthy, B. J. Currie, and S. F. Walton, 'Molecular characterisation of a pH-gated chloride channel from Sarcoptes scabiei', *Invertebr. Neurosci. IN*, vol. 7, no. 3, pp. 149–156, Sep. 2007.

[35] A. A. Beg, G. G. Ernstrom, P. Nix, M. W. Davis, and E. M. Jorgensen, 'Protons act as a transmitter for muscle contraction in C. elegans', *Cell*, vol. 132, no. 1, pp. 149–160, Jan. 2008.

[36] K. Schnizler *et al.*, 'A Novel Chloride Channel in Drosophila melanogaster Is Inhibited by Protons', *J. Biol. Chem.*, vol. 280, no. 16, pp. 16254–16262, Apr. 2005.

[37] A. N. Thompson, D. J. Posson, P. V. Parsa, and C. M. Nimigean, 'Molecular mechanism of pH sensing in KcsA potassium channels', *Proc. Natl. Acad. Sci. U. S. A.*, vol. 105, no. 19, pp. 6900–6905, May 2008.

[38] P. Holzer, 'Acid-sensitive ion channels and receptors', *Handb. Exp. Pharmacol.*, no. 194, pp. 283–332, 2009.

[39] I. Sazanavets and J. Warwicker, 'Computational Tools for Interpreting Ion Channel pH-Dependence', *PloS One*, vol. 10, no. 4, p. e0125293, 2015.

[40] Á. Nemecz, H. Hu, Z. Fourati, C. Van Renterghem, M. Delarue, and P.-J. Corringer, 'Full mutational mapping of titratable residues helps to identify proton-sensors involved in the control of channel gating in the Gloeobacter violaceus pentameric ligand-gated ion channel', *PLoS Biol.*, vol. 15, no. 12, p. e2004470, Dec. 2017.

[41] M. A. Alqazzaz, K. L. Price, and S. C. R. Lummis, 'Crotonic Acid Blocks the Gloeobacter Ligand-Gated Ion Channel (GLIC) via the Extracellular Domain', *Biochemistry*, vol. 55, no. 42, pp. 5947–5951, Oct. 2016.

[42] M. S. Prevost *et al.*, 'Identification of cinnamic acid derivatives as novel antagonists of the prokaryotic proton-gated ion channel GLIC', *J. Med. Chem.*, vol. 56, no. 11, pp. 4619–4630, Jun. 2013.

[43] H. Hu *et al.*, 'Crystal structures of a pentameric ion channel gated by alkaline pH show a widely open pore and identify a cavity for modulation', *Proc. Natl. Acad. Sci. U. S. A.*, vol. 115, no. 17, pp. E3959–E3968, Apr. 2018.

[44] W. Y. Lee and S. M. Sine, 'Principal pathway coupling agonist binding to channel gating in nicotinic receptors', *Nature*, vol. 438, no. 7065, pp. 243–247, Nov. 2005.

[45] Z. Fourati *et al.*, 'Structural Basis for a Bimodal Allosteric Mechanism of General Anesthetic Modulation in Pentameric Ligand-Gated Ion Channels', *Cell Rep.*, vol. 23, no. 4, pp. 993–1004, Apr. 2018.

[46] W. Zheng and A. Auerbach, 'Decrypting the Sequence of Structural Events during the Gating Transition of Pentameric Ligand-Gated Ion Channels Based on an Interpolated Elastic Network Model', *PLOS Comput. Biol.*, vol. 7, no. 1, p. e1001046, Jan. 2011.

[47] P. Purohit and A. Auerbach, 'Acetylcholine Receptor Gating: Movement in the α-Subunit Extracellular Domain', *J. Gen. Physiol.*, vol. 130, no. 6, pp. 569–579, Dec. 2007.

[48] S. Gupta, S. Chakraborty, R. Vij, and A. Auerbach, 'A mechanism for acetylcholine receptor gating based on structure, coupling, phi, and flip', *J. Gen. Physiol.*, vol. 149, no. 1, pp. 85–103, Jan. 2017.

[49] F. Zhu and G. Hummer, 'Drying Transition in the Hydrophobic Gate of the GLIC Channel Blocks Ion Conduction', *Biophys. J.*, vol. 103, no. 2, pp. 219–227, Jul. 2012.

[50] M. Cecchini and J.-P. Changeux, 'The nicotinic acetylcholine receptor and its prokaryotic homologues: Structure, conformational transitions & allosteric modulation', *Neuropharmacology*, vol. 96, no. Part B, pp. 137–149, Sep. 2015.

[51] N. E. Martin, S. Malik, N. Calimet, J.-P. Changeux, and M. Cecchini, 'Un-gating and allosteric modulation of a pentameric ligand-gated ion channel captured by molecular dynamics', *PLoS Comput. Biol.*, vol. 13, no. 10, p. e1005784, Oct. 2017.

[52] B. Lev *et al.*, 'String method solution of the gating pathways for a pentameric ligand-gated ion channel', *Proc. Natl. Acad. Sci. U. S. A.*, vol. 114, no. 21, pp. E4158–E4167, May 2017.

[53] D. Mowrey, Q. Chen, Y. Liang, J. Liang, Y. Xu, and P. Tang, 'Signal Transduction Pathways in the Pentameric Ligand-Gated Ion Channels', *PLOS ONE*, vol. 8, no. 5, p. e64326, May 2013.

[54] N. V. Di Russo, D. A. Estrin, M. A. Martí, and A. E. Roitberg, 'pH-Dependent conformational changes in proteins and their effect on experimental pK(a)s: the case of Nitrophorin 4', *PLoS Comput. Biol.*, vol. 8, no. 11, p. e1002761, 2012.

[55] I. Zimmermann, A. Marabelli, C. Bertozzi, L. G. Sivilotti, and R. Dutzler, 'Inhibition of the Prokaryotic Pentameric Ligand-Gated Ion Channel ELIC by Divalent Cations', *PLOS Biol.*, vol. 10, no. 11, p. e1001429, Nov. 2012.

[56] J. L. Galzi, S. Bertrand, P. J. Corringer, J. P. Changeux, and D. Bertrand, 'Identification of calcium binding sites that regulate potentiation of a neuronal nicotinic acetylcholine receptor.', *EMBO J.*, vol. 15, no. 21, pp. 5824–5832, Nov. 1996.

[57] A. M. Hosie, E. L. Dunne, R. J. Harvey, and T. G. Smart, 'Zinc-mediated inhibition of GABA(A) receptors: discrete binding sites underlie subtype specificity', *Nat. Neurosci.*, vol. 6, no. 4, pp. 362–369, Apr. 2003.

[58] F. Delbart *et al.*, 'An allosteric binding site of the α7 nicotinic acetylcholine receptor revealed in a humanized acetylcholine-binding protein', *J. Biol. Chem.*, vol. 293, no. 7, pp. 2534–2545, Feb. 2018.

[59] P. Velisetty, S. V. Chalamalasetti, and S. Chakrapani, 'Structural Basis for Allosteric Coupling at the Membrane-Protein Interface in Gloeobacter violaceus Ligand-gated Ion Channel (GLIC)', *J. Biol. Chem.*, vol. 289, no. 5, pp. 3013–3025, Jan. 2014.

[60] J. O. Schulze *et al.*, 'Bidirectional Allosteric Communication between the ATP-Binding Site and the Regulatory PIF Pocket in PDK1 Protein Kinase', *Cell Chem. Biol.*, vol. 23, no. 10, pp. 1193–1205, Oct. 2016.

[61] H. Nury *et al.*, 'Crystal structure of the extracellular domain of a bacterial ligand-gated ion channel', *J. Mol. Biol.*, vol. 395, no. 5, pp. 1114–1127, Feb. 2010.